Performance of the Vignale-Kohn functional in the linear response of metals

Berger, J. A.; Romaniello, P.; van Leeuwen, R.; de Boeij, P. L.

Published in:
Physical Review. B: Condensed Matter and Materials Physics

DOI:
10.1103/PhysRevB.74.245117

Publication date:
2006

Performance of the Vignale-Kohn functional in the linear response of metals

J. A. Berger, P. Romaniello, R. van Leeuwen, and P. L. de Boeij
Theoretical Chemistry, Materials Science Centre, Rijksuniversiteit Groningen, Nijenborgh 4, 9747 AG Groningen, The Netherlands
(Received 14 July 2006; revised manuscript received 15 October 2006; published 19 December 2006)

Recently the linear response of metallic solids has been formulated within the time-dependent current-density-functional approach [Romaniello and de Boeij, Phys. Rev. B **71**, 155108 (2005)]. The implementation, which originally used only the adiabatic local density approximation for the exchange-correlation kernel is extended in order to include also the Vignale-Kohn current functional. Within this approximation the exchange-correlation kernel is frequency dependent, thus relaxation effects due to electron-electron scattering can now be taken into account and some deficiencies of the adiabatic local density approximation (ALDA), as the absence of the low-frequency Drude-like tail in absorption spectra, can be cured. We strictly follow the previous formulation of the linear response of semiconductors by using the Vignale-Kohn functional [Berger, de Boeij, and van Leeuwen, Phys. Rev. B **71**, 155104 (2005)]. The self-consistent equations for the interband and intraband contributions to the induced density and current density, which are completely decoupled within the ALDA and in the long-wavelength limit, now remain coupled. We present our results calculated for the optical properties of the noble metals Cu, Ag, and Au and we compare them with measurements found in literature. In the case of Au we treat the dominant scalar relativistic effects using the zeroth-order regular approximation in the ground-state density-functional-theory calculations, as well as in the time-dependent response calculations.

DOI: 10.1103/PhysRevB.74.245117 PACS number(s): 71.45.Gm, 31.15.Ew, 78.20.−e, 78.66.Bz

I. INTRODUCTION

Recently the time-dependent current-density-functional theory (TDCDFT) formulation for the response of nonmetallic crystals[1,2] has been extended to treat metals.[3] In these systems one should not only consider the interband contribution to the response, involving transitions from (partially) occupied to (partially) unoccupied bands as in nonmetals, but also the intraband contribution due to transitions within the same band, more specifically, from just below the Fermi level to just above this level. The latter processes are responsible for the collective plasmon response typical for simple metallic systems.[4] We considered the linear response of the system to a general perturbation with wave vector $\mathbf{g}$ and frequency ω. We found that interband and intraband processes behave differently for small $\mathbf{g}$ and that the self-consistent-field equations for the interband and intraband contributions to the response decouple in the optical limit (vanishing $\mathbf{g}$ but finite ω) when we make use of the adiabatic local density approximation (ALDA). In this approximation the exchange-correlation scalar potential $v_{xc}(\mathbf{r},t)$ is just a local functional of the density. Within the ALDA this method yields good results for the dielectric and the electron energy loss functions of several transition metals. However the adiabatic approximation fails in describing the low-frequency Drude-like absorption, which is missing in all the calculated absorption spectra. This absorption is due to relaxation processes such as electron-electron and electron-phonon scattering. The description of the electron-phonon interaction requires the use of a multicomponent-density functional approach.[5,6] The electron-electron scattering can be described within our method by using more advanced exchange-correlation functionals where a frequency-dependent exchange-correlation kernel is used.

In this work we go beyond the ALDA and we employ an exchange-correlation vector potential, $\mathbf{A}_{xc}(\mathbf{r},t)$, which we approximate as a local functional of the current density using the expression derived by Vignale and Kohn.[7,8] The evaluation of the Vignale-Kohn (VK) expression requires knowledge of some properties of the homogeneous electron gas, i.e., the exchange-correlation energy per unit volume, $\epsilon_{xc}^{h}(\rho)$, and the longitudinal and transverse exchange-correlation kernels, $f_{xcL}^{h}(\rho,\omega)$ and $f_{xcT}^{h}(\rho,\omega)$, respectively, where ρ is the electron density of the electron gas. Knowledge of the first is already required in the ALDA and can be obtained from the accurate results of Monte Carlo calculations.[9,10] The exchange-correlation kernels, on the other hand, are not known accurately. There are two works in which parametrizations are given for both $f_{xcL}^{h}(\rho,\omega)$ and $f_{xcT}^{h}(\rho,\omega)$. One is by Conti, Nifosì, and Tosi (CNT) (Ref. 11) and the other is by Qian and Vignale (QV).[12] An important difference between the parametrizations of CNT and QV occurs in the $\omega\rightarrow 0$ limit of $f_{xcT}^{h}(\rho,\omega)$. Whereas $f_{xcT}^{h}(\rho,\omega)$ of CNT vanishes in that limit, the QV parametrization does not, i.e., it has a small but finite value. The fact that $f_{xcT}^{h}(\rho,\omega)$ vanishes in the $\omega\rightarrow 0$ limit in the case of the CNT parametrization has the important consequence that the VK expression for $\delta\mathbf{A}_{xc}(\mathbf{r},\omega)$ reduces to that of the ALDA in that limit. The value of $f_{xcT}^{h}(\rho,0)$ is related to μ_{xc}, the exchange-correlation part of the shear modulus, a quantity that is known only approximately. In previous work we showed that it is this difference in behavior of the two parametrizations in the zero-frequency limit that leads to very different absorption spectra of infinite polymer chains and bulk semiconductors.[13,14] Whereas spectra obtained with the CNT parametrization are relatively close to spectra obtained within the ALDA, spectra obtained with the QV parametrization are very different from the ALDA results and from the experiments. Since QV give an expression for their parametrization in which $f_{xcL,T}^{h}(\rho,0)$ enter, their parametrization can easily be adapted for the case $f_{xcT}^{h}(\rho,0)=0$. With the resulting parametrization we obtained absorption spectra for silicon that are again close to the spec-

tra obtained with the CNT parametrization and those obtained within the ALDA.[13,14] In view of the obtained results mentioned above and the fact that we are mainly interested in the frequency dependence of the VK functional in order to describe relaxation effects due to electron-electron scattering we choose to enforce continuity with the ALDA in the limit $\omega \to 0$ by setting $f^h_{xcT}(\rho,0)=0$ also in the QV parametrization. Furthermore, we will show that only in the case that $f^h_{xcT}(\rho,0)=0$ the VK functional leads to optical spectra with the correct ω dependence in the limit of $\omega \to 0$. We explicitly checked that finite values for $f^h_{xcT}(\rho,0)$ lead to the same deficiencies in the optical spectra of metals as in those of semiconductors.[14]

The outline of this paper is as follows. In Sec. II we start by giving a description of the theory we use. We first give an introduction to TDCDFT and its application in the linear response regime. Then we introduce the self-consistent set of equations which describe the linear response of metallic crystals. Furthermore, we introduce the VK functional and discuss the parametrizations of the exchange-correlation kernels of the homogeneous electron gas $f^h_{xcL,T}(\rho,\omega)$ that enter the VK functional. At the end of the section we give the main equations we use to treat the dominant scalar relativistic effects within the zeroth order regular approximation (ZORA). We will use the ZORA to describe the scalar relativistic effects in Au. We report the main aspects of the implementation in Sec. III. In Sec. IV we show our results for the dielectric and electron energy loss functions of the crystals of Cu, Ag, and Au, and we compare them with the best available experimental data[15–22] and the best theoretical data.[23,24] Finally, we give our conclusions in Sec. V.

II. THEORY

A. Time-dependent current-density-functional theory

It was shown by Runge and Gross[25] that, for a given initial state, there is a one-to-one correspondence between the time-dependent density $\rho(\mathbf{r},t)$ and the time-dependent external scalar potential $v(\mathbf{r},t)$ up to a purely additive time-dependent function $c(t)$. Ghosh and Dhara[26,27] extended the Runge-Gross proof to systems subjected to general time-dependent electromagnetic fields by proving that, for a given initial state, there exists a one-to-one correspondence up to a gauge transformation between the time-dependent current density and the set of potentials $\{v(\mathbf{r},t),\mathbf{A}(\mathbf{r},t)\}$, in which $\mathbf{A}(\mathbf{r},t)$ is the time-dependent external vector potential (see also Refs. 28 and 29). Ghosh and Dhara further provide a practical scheme for calculating time-dependent densities and current densities. Here an interacting many-particle system in an external electromagnetic field is replaced by an auxiliary noninteracting many-particle system in an effective field desribed by the set of Kohn-Sham potentials $\{v_s(\mathbf{r},t),\mathbf{A}_s(\mathbf{r},t)\}$.[30] This set of potentials has the property that, for a given initial state, it produces the exact time-dependent current density and the exact time-dependent density. If the initial state is the ground state, it is already determined by the ground-state density on the basis of the Hohenberg-Kohn theorem.[31] This time-dependent Kohn-Sham theory was later strengthened by a generalization of the Runge-Gross theorem by Vignale who showed that under some assumptions such a set of potentials indeed exists and is unique.[29] In the Kohn-Sham scheme the time-dependent single-particle wave functions are solutions of the following equation [we use atomic units ($e=\hbar=m=1$) throughout the paper]:

$$i\frac{\partial}{\partial t}\phi_n(\mathbf{r},t)=\left(\frac{1}{2}[\hat{\mathbf{p}}+\mathbf{A}_s(\mathbf{r},t)]^2+v_s(\mathbf{r},t)\right)\phi_n(\mathbf{r},t), \quad (1)$$

where $\hat{\mathbf{p}}=-i\nabla$ is the momentum operator. Given the initial state, the time-dependent potentials $v_s(\mathbf{r},t)$ and $\mathbf{A}_s(\mathbf{r},t)$ produce the exact time-dependent density and current density,

$$\rho(\mathbf{r},t)=\sum_n f_n\phi_n^*(\mathbf{r},t)\phi_n(\mathbf{r},t), \quad (2)$$

$$\mathbf{j}(\mathbf{r},t)=\sum_n f_n\,\mathrm{Re}[-i\phi_n^*(\mathbf{r},t)\,\nabla\,\phi_n(\mathbf{r},t)]+\rho(\mathbf{r},t)\mathbf{A}_s(\mathbf{r},t), \quad (3)$$

where f_n are the occupation numbers given by the Fermi-Dirac distribution function at zero temperature, i.e., $f_n=f(\epsilon_n)=2$ for $\epsilon_n \leqslant \epsilon_F$ and 0 otherwise, with ϵ_n the ground state orbital energies and ϵ_F the Fermi energy. Here we assumed that our initial state is nondegenerate and is described by a single Slater determinant. The first and second terms on the right-hand side of Eq. (3) correspond to the paramagnetic and diamagnetic current, respectively. Both the density and the current density are gauge invariant.

In this paper we treat the dynamic linear response of a metallic solid to a macroscopic field within TDCDFT. A time-dependent electric field $\mathbf{E}_{\mathrm{ext}}(\mathbf{r},t)$ applied to a solid at a time $t=t_0$ will induce a macroscopic polarization $\mathbf{P}_{\mathrm{mac}}(\mathbf{r},t)$. For a uniform external field the macroscopic polarization can be obtained from the induced current density by

$$\mathbf{P}_{\mathrm{mac}}(t)=\frac{-1}{V}\int_{t_0}^{t}\int_V \delta\mathbf{j}(\mathbf{r},t')d\mathbf{r}dt', \quad (4)$$

where V is the volume of a unit cell. This polarization is proportional to the macroscopic field $\mathbf{E}_{\mathrm{mac}}(t)$, comprising both the external and the average induced field within the solid,

$$\mathbf{P}_{\mathrm{mac}}(t)=\int_{t_0}^{t}\chi_e(t-t')\cdot\mathbf{E}_{\mathrm{mac}}(t')dt'. \quad (5)$$

Here the constant of proportionality $\chi_e(t-t')$ is the electric susceptibity, which, unlike $\mathbf{P}_{\mathrm{mac}}(t)$ and $\mathbf{E}_{\mathrm{mac}}(t)$, is a bulk property of the system since it is independent of its shape and size.

B. Linear response

The first-order perturbation of the ground state is governed by the perturbation Hamiltonian $\delta\hat{H}_s$ containing all terms linear in the field,

$$\delta\hat{H}_s(\mathbf{r},t) = \tfrac{1}{2}[\hat{\mathbf{p}}\cdot\delta\mathbf{A}_s(\mathbf{r},t) + \delta\mathbf{A}_s(\mathbf{r},t)\cdot\hat{\mathbf{p}}] + \delta v_s(\mathbf{r},t). \quad (6)$$

We choose the gauge to be the microscopic Coulomb gauge of Kootstra *et al.*[1] in which the Kohn-Sham scalar and vector potentials are given by

$$\delta v_s(\mathbf{r},t) = \delta v_{H,\mathrm{mic}}(\mathbf{r},t) + \delta v_{xc,\mathrm{mic}}(\mathbf{r},t), \quad (7)$$

$$\delta\mathbf{A}_s(\mathbf{r},t) = \delta\mathbf{A}_{\mathrm{mac}}(\mathbf{r},t) + \delta\mathbf{A}_{xc}(\mathbf{r},t). \quad (8)$$

Here $\delta v_{H,\mathrm{mic}}(\mathbf{r},t)$ is the microscopic part of the Hartree potential and $\delta v_{xc,\mathrm{mic}}(\mathbf{r},t)$ is the microscopic part of the exchange-correlation potential. The term $\delta\mathbf{A}_{\mathrm{mac}}(\mathbf{r},t)$ denotes the macroscopic vector potential,

$$\delta\mathbf{A}_{\mathrm{mac}}(\mathbf{r},t) = \delta\mathbf{A}_{\mathrm{ext}}(\mathbf{r},t) + \delta\mathbf{A}_{\mathrm{ind}}(\mathbf{r},t), \quad (9)$$

where $\delta\mathbf{A}_{\mathrm{ext}}(\mathbf{r},t)$ is the external vector potential and $\delta\mathbf{A}_{\mathrm{ind}}(\mathbf{r},t)$ is the induced macroscopic vector potential. The latter potential accounts for the long-range contribution of the Hartree potential of the surface charge as well as the retarded contribution of the induced transverse current density. We can neglect the microscopic part of the vector potential which is consistent with the Breit approximation used in the ground state calculation.[1,32,33] We choose the field $\mathbf{E}_{\mathrm{mac}}(\mathbf{r},t)$ to be fixed and its relation to $\delta\mathbf{A}_{\mathrm{mac}}(\mathbf{r},t)$ is given by $\partial_t\delta\mathbf{A}_{\mathrm{mac}}(\mathbf{r},t) = -\mathbf{E}_{\mathrm{mac}}(\mathbf{r},t)$. We leave the relation between $\mathbf{E}_{\mathrm{mac}}(\mathbf{r},t)$ and $\mathbf{E}_{\mathrm{ext}}(t)$ unspecified as this depends on the sample size and shape and requires knowledge of χ_e. Finally, $\delta\mathbf{A}_{xc}(\mathbf{r},t)$ is the exchange-correlation vector potential. In practice approximations are required for the exchange-correlation potentials $\delta v_{xc}(\mathbf{r},t)$ and $\delta\mathbf{A}_{xc}(\mathbf{r},t)$.

In a recent work[3] $\delta v_{xc}^{\mathrm{ALDA}}(\mathbf{r},t)$ was used for the exchange-correlation scalar potential and the exchange-correlation vector potential was neglected. In this case the Kohn-Sham vector potential is completely determined by the macroscopic electric field which is kept fixed. We then only need to solve the equation for the induced density self-consistently, and afterwards the induced current density can be calculated. Approximations beyond the ALDA imply a self-consistent solution of the equations for both the induced density and induced current density, which will remain coupled.

To study the linear response properties of systems, which are initially in the ground state and perturbed by a time-dependent electromagnetic field, it is convenient to work in the frequency domain. To do this we use a Fourier transformation defined by

$$\delta\tilde{\mathbf{A}}_s(\mathbf{r},\omega) = \int \delta\mathbf{A}_s(\mathbf{r},t)e^{i\omega t}d\omega. \quad (10)$$

For notational convenience we will drop the tilde on $\delta\tilde{\mathbf{A}}(\mathbf{r},\omega)$ in the following and assume that it is clear from the frequency dependence that we are dealing with a different quantity. We consider a general perturbation characterized by the wave vector $\mathbf{g}$ and frequency ω according to

$$\delta\mathbf{A}_s(\mathbf{r},\omega) = e^{i\mathbf{g}\cdot\mathbf{r}}\delta\mathbf{A}_{\mathbf{g},s}(\mathbf{r},\omega), \quad (11)$$

where $\delta\mathbf{A}_{\mathbf{g},s}(\mathbf{r},\omega)$ is lattice periodic, i.e.,

$$\delta\mathbf{A}_{\mathbf{g},s}(\mathbf{r},\omega) = \delta\mathbf{A}_{\mathbf{g},s}(\mathbf{r}+\mathbf{R},\omega), \quad (12)$$

with $\mathbf{R}$ a Bravais lattice vector. We choose the perturbation to be real and therefore we have

$$\delta\mathbf{A}_{\mathbf{g},s}(\mathbf{r},\omega) = \delta\mathbf{A}^*_{-\mathbf{g},s}(\mathbf{r},-\omega). \quad (13)$$

We have similar expressions for the scalar potential.

We are interested in the linear response of the system for vanishing $\mathbf{g}$ but finite ω, which is the regime describing optical properties. An essential point of our formulation is that interband and intraband processes behave differently for small $\mathbf{g}$. It can be shown that within the linear response regime the induced density and induced current density can be written as[3]

$$\delta\rho(\mathbf{r},\omega) = e^{i\mathbf{g}\cdot\mathbf{r}}\delta\rho_{\mathbf{g}}(\mathbf{r},\omega), \quad (14)$$

$$\delta\mathbf{j}(\mathbf{r},\omega) = e^{i\mathbf{g}\cdot\mathbf{r}}\delta\mathbf{j}_{\mathbf{g}}(\mathbf{r},\omega), \quad (15)$$

where $\delta\rho_{\mathbf{g}}(\mathbf{r},\omega)$ and $\delta\mathbf{j}_{\mathbf{g}}(\mathbf{r},\omega)$ are lattice periodic. In order to show that interband and intraband processes behave differently for small $\mathbf{g}$ we split $\delta\rho_{\mathbf{g}}(\mathbf{r},\omega)$ and $\delta\mathbf{j}_{\mathbf{g}}(\mathbf{r},\omega)$ into their contributions from interband and intraband processes and evaluate these contributions separately. We therefore write

$$\delta\rho_{\mathbf{g}}(\mathbf{r},\omega) = \delta\rho_{\mathbf{g}}^{\mathrm{inter}}(\mathbf{r},\omega) + \delta\rho_{\mathbf{g}}^{\mathrm{intra}}(\mathbf{r},\omega), \quad (16)$$

$$\delta\mathbf{j}_{\mathbf{g}}(\mathbf{r},\omega) = \delta\mathbf{j}_{\mathbf{g}}^{\mathrm{inter}}(\mathbf{r},\omega) + \delta\mathbf{j}_{\mathbf{g}}^{\mathrm{intra}}(\mathbf{r},\omega). \quad (17)$$

For finite $\mathbf{g}$ the lattice periodic density $\delta\rho_{\mathbf{g}}(\mathbf{r},\omega)$ and lattice periodic current density $\delta\mathbf{j}_{\mathbf{g}}(\mathbf{r},\omega)$ can be written in terms of the lattice periodic potentials and Kohn-Sham response functions. We give these expressions in the following concise form:

$$\begin{pmatrix} \delta\rho_{\mathbf{g}}^{\mathrm{inter}} \\ i\delta\mathbf{j}_{\mathbf{g}}^{\mathrm{inter}}/\omega \end{pmatrix} = \begin{pmatrix} \chi_{\rho\rho,\mathbf{g}}^{\mathrm{inter}} & -i\chi_{\rho\mathbf{j}_p,\mathbf{g}}^{\mathrm{inter}}/\omega \\ i\chi_{\mathbf{j}_p\rho,\mathbf{g}}^{\mathrm{inter}}/\omega & \Delta\chi_{\mathbf{j}_p\mathbf{j}_p,\mathbf{g}}^{\mathrm{inter}}/\omega^2 \end{pmatrix} \begin{pmatrix} \delta v_{\mathbf{g},s} \\ i\omega\delta\mathbf{A}_{\mathbf{g},s} \end{pmatrix}, \quad (18)$$

for the interband contributions, and

$$i\omega\begin{pmatrix} \omega/g\,\delta\rho_{\mathbf{g}}^{\mathrm{intra}} \\ \delta\mathbf{j}_{\mathbf{g}}^{\mathrm{intra}} \end{pmatrix} = \begin{pmatrix} \omega^2/g^2\chi_{\rho\rho,\mathbf{g}}^{\mathrm{intra}} & \omega/g\chi_{\rho\mathbf{j}_p,\mathbf{g}}^{\mathrm{intra}} \\ \omega/g\chi_{\mathbf{j}_p\rho,\mathbf{g}}^{\mathrm{intra}} & \Delta\chi_{\mathbf{j}_p\mathbf{j}_p,\mathbf{g}}^{\mathrm{intra}} \end{pmatrix} \begin{pmatrix} ig\,\delta v_{\mathbf{g},s} \\ i\omega\delta\mathbf{A}_{\mathbf{g},s} \end{pmatrix}, \quad (19)$$

for the intraband part. We note that the matrix vector products in the above expressions include an integration over a real-space coordinate. Furthermore we defined

$$\Delta\chi_{\mathbf{j}_p\mathbf{j}_p,\mathbf{g}} = \chi_{\mathbf{j}_p\mathbf{j}_p,\mathbf{g}}(\mathbf{r},\mathbf{r}',\omega) - \chi_{\mathbf{j}_p\mathbf{j}_p,\mathbf{g}}(\mathbf{r},\mathbf{r}',\omega=0), \quad (20)$$

where the Kohn-Sham response function $\chi_{\mathbf{j}_p\mathbf{j}_p,\mathbf{g}}(\omega)$ at $\omega=0$ enters our expressions because we have made use of the conductivity sum rule given by

$$[\chi_{\mathbf{j}_p\mathbf{j}_p}(\mathbf{r},\mathbf{r}',0)]_{ij} + \rho_0(\mathbf{r})\delta_{ij}\delta(\mathbf{r}-\mathbf{r}') = 0, \quad (21)$$

which is convenient in practical applications. However, this means that we neglect the small Landau diamagnetic contribution for the transverse component of the induced current density.[4] We note that the terms appearing on the left-hand

sides of Eqs. (18) and (19) are all of order 1. The Kohn-Sham response functions that enter the above expressions are given by

$$\chi_{ab,\mathbf{g}}(\mathbf{r},\mathbf{r}',\omega)=\frac{1}{N_k}\lim_{\eta\to 0^+}\sum_{\mathbf{k}}\sum_{n,n'}\frac{(f_{n\mathbf{k}}-f_{n'\mathbf{k}+\mathbf{g}})}{1+\delta_{n,n'}}\times\frac{[\phi^*_{n\mathbf{k}}(\mathbf{r})\tilde{a}_{\mathbf{g}}\phi_{n'\mathbf{k}+\mathbf{g}}(\mathbf{r})][\phi^*_{n'\mathbf{k}+\mathbf{g}}(\mathbf{r}')\tilde{b}_{-\mathbf{g}}\phi_{n\mathbf{k}}(\mathbf{r}')]}{\omega-(\epsilon_{n'\mathbf{k}+\mathbf{g}}-\epsilon_{n\mathbf{k}})+i\eta} \tag{22}$$

in which $\tilde{a}_{\mathbf{g}}$ and $\tilde{b}_{\mathbf{g}}$ can be either $\tilde{\rho}_{\mathbf{g}}=e^{-i\mathbf{g}\cdot\mathbf{r}}$ or $\tilde{\mathbf{j}}_{p,\mathbf{g}}=-i(e^{-i\mathbf{g}\cdot\mathbf{r}}\nabla-\nabla^{\dagger}e^{-i\mathbf{g}\cdot\mathbf{r}})/2$, where the dagger on the nabla operator indicates that it acts on terms to the left of it. In Eq. (22) ϵ_n are the eigenvalues of the Kohn-Sham orbitals ϕ_n of the unperturbed system. The positive infinitesimal η in Eq. (22) ensures the causality of the response function. The Bloch functions are normalized on the Wigner-Seitz cell with volume V_{WS}, and the number of $\mathbf{k}$ points in the summation is $N_k=V_{BvK}/V_{\mathrm{WS}}$, in which V_{BvK} is the volume of the Born-von Kármán cell. The intraband (interband) contribution to the response functions is given by the terms with $n=n'$ ($n\neq n'$) in the summation over n and n'. In the intraband case the factor $1/(1+\delta_{n,n'})$ corrects for the double counting.

The various interband contributions to the response functions given in Eq. (18) have the following ω dependence:[3]

$$\chi^{\mathrm{inter}}_{\rho\rho,\mathbf{g}}\propto 1,$$

$$\chi^{\mathrm{inter}}_{\rho\mathbf{j}_p,\mathbf{g}},\chi^{\mathrm{inter}}_{\mathbf{j}_p\rho,\mathbf{g}}\propto\omega,$$

$$\Delta\chi^{\mathrm{inter}}_{\mathbf{j}_p\mathbf{j}_{p'},\mathbf{g}}\propto\omega^2, \tag{23}$$

whereas the intraband response functions given in Eq. (19) have the following ω and g dependence at small $\mathbf{g}$ but finite ω,[3]

$$\chi^{\mathrm{intra}}_{\rho\rho,\mathbf{g}}\propto g^2/\omega^2,$$

$$\chi^{\mathrm{intra}}_{\rho\mathbf{j}_{p'},\mathbf{g}},\chi^{\mathrm{intra}}_{\mathbf{j}_p\rho,\mathbf{g}}\propto g/\omega,$$

$$\Delta\chi^{\mathrm{intra}}_{\mathbf{j}_p\mathbf{j}_{p'},\mathbf{g}}\propto 1. \tag{24}$$

Therefore the terms that enter the matrices in Eqs. (18) and (19) are all of order 1. This means that according to Eq. (19) in the limit $\mathbf{g}\to 0$ the Kohn-Sham scalar potential does not contribute to the intraband contribution to the induced density and current density. Only the Kohn-Sham vector potential contributes to the intraband contribution to the induced density and current density. Since the Kohn-Sham vector potential itself depends on the total induced current density, i.e., the sum of the interband and intraband contributions, the set of self-consistent equations for the interband and intraband contributions to the density and current density are coupled. From the induced current density obtained from this self-consistent scheme we can obtain the electric susceptibility χ_e from Eqs. (4) and (5) which within the linear response regime can be rewritten as

$$\mathbf{P}_{\mathrm{mac}}(\omega)=\frac{-i}{\omega V}\int_V\delta\mathbf{j}(\mathbf{r},\omega)d\mathbf{r} \tag{25}$$

and

$$\mathbf{P}_{\mathrm{mac}}(\omega)=\chi_e(\omega)\cdot\mathbf{E}_{\mathrm{mac}}(\omega). \tag{26}$$

C. The Vignale-Kohn functional

The general expression for the exchange-correlation vector potential is to first order

$$\delta A_{xc,i}(\mathbf{r},\omega)=\sum_j\int d\mathbf{r}'f_{xc,ij}(\mathbf{r},\mathbf{r}',\omega)\delta j_j(\mathbf{r}',\omega). \tag{27}$$

This expression defines the tensor kernel $\overleftrightarrow{f}_{xc}(\mathbf{r},\mathbf{r}',\omega)$. Vignale and Kohn derived an approximation for $\delta\mathbf{A}_{xc}(\mathbf{r},\omega)$ (Refs. 7 and 8) by studying a periodically modulated electron gas with wave vector $\mathbf{q}$ under the influence of an external perturbation with wave vector $\mathbf{k}$. This expression was proved to be valid if $k,q\ll k_F,\omega/v_F$, where k_F and v_F are the Fermi momentum and the Fermi velocity, respectively. By construction the VK functional obeys several exact constraints. The VK functional satisfies the zero-force and zero-torque constraints which state that the exchange-correlation potentials cannot exert a net force or a net torque on the system. Furthermore, it obeys the requirement of generalized translational invariance which states that a rigid translation of the current density implies a rigid translation of the exchange-correlation potentials. Finally, it satisfies the Onsager symmetry relation which restricts the form of exchange-correlation kernel $\overleftrightarrow{f}_{xc}(\mathbf{r},\mathbf{r}',\omega)$. Vignale, Ullrich, and Conti showed that the complicated VK expression for $\delta\mathbf{A}_{xc}(\mathbf{r},\omega)$ could be written in the following physically transparent form:[34]

$$i\omega\delta A_{xc,i}(\mathbf{r},\omega)=\partial_i\delta v^{\mathrm{ALDA}}_{xc}(\mathbf{r},\omega)-\frac{1}{\rho_0(\mathbf{r})}\sum_j\partial_j\sigma_{xc,ij}(\mathbf{r},\omega), \tag{28}$$

where the first term on the right-hand side is just the linearization of the ALDA exchange-correlation scalar potential. Using a gauge transform this longitidinal part of $\delta\mathbf{A}_{xc}(\mathbf{r},\omega)$ can be included in the scalar potential. The second term is the divergence of a tensor field $\overleftrightarrow{\sigma}_{xc}(\mathbf{r},\omega)$ which has the structure of a symmetric viscoelastic stress tensor,

$$\sigma_{xc,ij}=\tilde{\eta}_{xc}\left(\partial_ju_i+\partial_iu_j-\frac{2}{3}\delta_{ij}\sum_k\partial_ku_k\right)+\tilde{\zeta}\delta_{ij}\sum_k\partial_ku_k \tag{29}$$

in which the velocity field $\mathbf{u}(\mathbf{r},\omega)$ is given by

$$\mathbf{u}(\mathbf{r},\omega)=\frac{\delta\mathbf{j}(\mathbf{r},\omega)}{\rho_0(\mathbf{r})}. \tag{30}$$

The coefficients $\tilde{\eta}_{xc}(\mathbf{r},\omega)$ and $\tilde{\zeta}_{xc}(\mathbf{r},\omega)$ are determined by the longitudinal and transverse response kernels of the homogeneous electron gas evaluated at the density $\rho_0(\mathbf{r})$,

$$\tilde{\eta}_{xc}(\mathbf{r},\omega) = \frac{i}{\omega}\rho_0^2(\mathbf{r}) f_{xcT}^h(\rho_0(\mathbf{r}),\omega), \tag{31}$$

and

$$\tilde{\zeta}_{xc}(\mathbf{r},\omega) = \frac{i}{\omega}\rho_0^2(\mathbf{r})\left(f_{xcL}^h(\rho_0(\mathbf{r}),\omega) - \frac{4}{3}f_{xcT}^h(\rho_0(\mathbf{r}),\omega) - \frac{d^2\epsilon_{xc}^h}{d\rho^2}[\rho_0(\mathbf{r})]\right), \tag{32}$$

where $\epsilon_{xc}^h(\rho)$ is the exchange-correlation energy per unit volume of the homogeneous electron gas. The quantities $\tilde{\eta}_{xc}(\mathbf{r},\omega)$ and $\tilde{\zeta}_{xc}(\mathbf{r},\omega)$ can be interpreted as viscoelastic coefficients.[34,36] The coefficients $f_{xcL,T}^h(\omega)$ are defined by the identity[8,35]

$$f_{xcL,T}^h(\omega) \equiv \lim_{\mathbf{k}\to 0} f_{xcL,T}^h(\mathbf{k},\omega). \tag{33}$$

Unfortunately the longitudinal and transverse exchange-correlation kernels are not known accurately. However, they have been extensively studied and some exact features are well known.[11,12,36–38] In particular Conti and Vignale[36] obtained the exact results for $\lim_{\omega\to 0}\lim_{\mathbf{k}\to 0} f_{xcL,T}^h(\mathbf{k},\omega)$ by comparing the microscopic linear-response equations with the macroscopic viscoelastic equation of motion. Their evaluations led to the following identities for the three-dimensional electron gas:

$$\lim_{\omega\to 0}\lim_{\mathbf{k}\to 0} f_{xcL}^h(\mathbf{k},\omega) = \frac{1}{\rho^2}\left(K_{xc} + \frac{4}{3}\mu_{xc}\right), \tag{34}$$

$$\lim_{\omega\to 0}\lim_{\mathbf{k}\to 0} f_{xcT}^h(\mathbf{k},\omega) = \frac{\mu_{xc}}{\rho^2}, \tag{35}$$

where K_{xc} and μ_{xc} are the exchange-correlation parts of the bulk and shear modulus, respectively, which are real quantities. Since $K_{xc}=\rho^2[d^2\epsilon_{xc}^h(\rho)/d\rho^2]$ we see from Eqs. (34) and (35) that the parameter $\tilde{\zeta}_{xc}(\mathbf{r},\omega)$ contains a factor for which one can prove the exact relation[34,36]

$$\lim_{\omega\to 0}\left(f_{xcL}^h(\rho(\mathbf{r}),\omega) - \frac{4}{3}f_{xcT}^h(\rho(\mathbf{r}),\omega) - \frac{d^2\epsilon_{xc}^h}{d\rho^2}[\rho(\mathbf{r})]\right) = 0. \tag{36}$$

From the above relations we can determine the behavior of the coefficients $\tilde{\eta}_{xc}(\mathbf{r},\omega)$ and $\tilde{\zeta}_{xc}(\mathbf{r},\omega)$ in the limit $\omega\to 0$. We obtain

$$\lim_{\omega\to 0}\frac{-i\omega\tilde{\zeta}_{xc}(\mathbf{r},\omega)}{\rho_0^2(\mathbf{r})} = 0, \tag{37}$$

$$\lim_{\omega\to 0}\frac{-i\omega\tilde{\eta}_{xc}(\mathbf{r},\omega)}{\rho_0^2(\mathbf{r})} = f_{xcT}(\rho_0(\mathbf{r}),0). \tag{38}$$

We see that only if $\mu_{xc}=0$ the VK expression (28) reduces to the ALDA in the limit $\omega\to 0$, otherwise it does not. The exchange-correlation part of the shear modulus can be related to the Landau parameters F_l as[36]

$$\mu_{xc} = \frac{2\rho\epsilon_F}{5}\frac{F_2/5 - F_1/3}{1+F_1/3}. \tag{39}$$

The bulk modulus $K_{xc}=\rho^2[d^2\epsilon_{xc}^h(\rho)/d\rho^2]$ can be obtained from accurate results of Monte Carlo calculations.[9,10] The shear modulus μ_{xc}, however, is not accurately known. Values for μ_{xc} can be obtained from the calculations performed by Nifosì, Conti, and Tosi[38] or from Eq. (39) using the Landau parameters calculated by Yasuhara and Ousaka.[12,36,39] Even though the results may not be accurate, it is clear from these calculations that μ_{xc} is much smaller than K_{xc}. Surprisingly, however, it turns out that μ_{xc} has a much bigger influence than K_{xc} on the optical spectra of infinite polymer chains and bulk semiconductors leading to a collapse of these spectra.[13,14] If we make the approximation $\mu_{xc}=0$ we obtain results close to the results obtained within the ALDA, since in this approximation the VK expression, Eq. (28), reduces to the ALDA in the limit $\omega\to 0$ and the values of the coefficients $f_{xcL,T}^h(\omega)$ are close to $f_{xcL,T}^h(0)$ for $\omega\ll\omega_{pl}$ which is the range of frequencies that were interested in.

Finally, let us briefly discuss the two parametrizations that exist for $f_{xcL,T}^h(\omega)$ and that we will use in this chapter. Conti, Nifosì and Tosi (CNT) (Ref. 11) calculated $\mathrm{Im}\, f_{xcL,T}^h(\omega)$ directly by means of an approximate decoupling of an exact four-point response function. CNT then introduced parametrizations for $\mathrm{Im}\, f_{xcL,T}^h(\omega)$ that reproduce their numerical results. The real part can then be obtained from the Kramers-Krönig dispersion relations. Their results have the correct behavior in the limit $\omega\to\infty$, the high-frequency limit of $\mathrm{Im} f_{xcL}^h(\omega)$ being equal to that obtained by Glick and Long.[40] The real parts of $f_{xcL,T}^h(\omega)$ can be obtained from the Kramers-Krönig dispersion relations where the high-frequency limits of $f_{xcL,T}^h(\omega)$ were obtained from third-frequency-moment sum rules.[36,41–43] However, their results do not reduce to the exact results in the limit $\omega\to 0$ given in Eqs. (34) and (35) because they invoke the compressibility sum rule,

$$\lim_{\mathbf{k}\to 0}\lim_{\omega\to 0} f_{xcL}^h(\mathbf{k},\omega) = \frac{K_{xc}}{\rho^2}, \tag{40}$$

thereby interchanging the order of the limits with respect to the exact result (34). This is equivalent to the approximation $\mu_{xc}=0$. Because of the uncertainty in the precise values of μ_{xc}, the fact that it is small compared to K_{xc} and the appeal of a theory that reduces to the ALDA in the limit $\omega\to 0$ CNT prefer to enforce equality of the order of limits.[11] A distinct feature of the CNT result is a pronounced peak around $\omega=2\omega_{pl}$ in $\mathrm{Im}\, f_{xcL,T}^h(\omega)$, where ω_{pl} is the plasmon frequency.

An alternative parametrization was given by Qian and Vignale.[12] First they obtained an exact result for the slope of $\mathrm{Im}\, f_{xcL,T}^h(\omega)$ at $\omega=0$. Then they adopt an interpolation formula first introduced by Gross and Kohn[42] to model $\mathrm{Im}\, f_{xcL,T}^h(\omega)$. To satisfy the constraint on the slope of $\mathrm{Im}\, f_{xcL,T}^h(\omega)$ at $\omega=0$ they need one more parameter. This extra parameter in their scheme is the width of a Gaussian peak around $\omega=2\omega_{pl}$ that accounts for the two-plasmon contributions found by CNT. The coefficients in their interpolation formula are then chosen such to reproduce the correct behavior in the limit $\omega\to\infty$ as well as the correct behavior in the

limit $\omega \to 0$ determined by their result for the slope of $\mathrm{Im}\, f^h_{xcL,T}(\omega)$ at $\omega=0$ and Eqs. (34) and (35). Their model shows a peak that is less pronounced than CNT's. Since QV give an expression for their parametrization in which $f^h_{xcL,T}(0)$ enter explicitly, their parametrization can easily be adapted for the case $f^h_{xcT}(0)=0$. For reasons mentioned in the Introduction we, like CNT, prefer to use a theory that reduces to the ALDA in the limit $\omega \to 0$. This means that we will use the QV parametrization only with $f^h_{xcT}(0)=0$ (i.e., $\mu_{xc}=0$). We will denote this approximation by QVA.

D. Relativistic corrections

In the case of Au we include scalar relativistic effects in our formulation by using the zeroth-order regular approximation (ZORA)[44–46] along the same line as described in Refs. 47–49 and 57. We use the the ground-state ZORA equation,

$$\left(\hat{\mathbf{g}} \cdot \frac{K(\mathbf{r})}{2}\hat{\mathbf{g}} + v_{s,0}(\mathbf{r})\right)\phi_{i\mathbf{g}}(\mathbf{r}) = \epsilon_{i\mathbf{g}}\phi_{i\mathbf{g}}(\mathbf{r}), \tag{41}$$

to get the orbitals and the orbital energies needed in Eq. (22) to calculate the response functions. Here $v_{s,0}(\mathbf{r})$ is the self-consistent Kohn-Sham potential of the ground state and the factor $K(\mathbf{r})$ is given by

$$K(\mathbf{r}) = \frac{2c^2}{2c^2 - v_{s,0}(\mathbf{r})}, \tag{42}$$

where c is the velocity of light. The time-dependent Hamiltonian including scalar relativistic effects within the ZORA is given by

$$\hat{H}^{\mathrm{ZORA}}(t) = \hat{\pi}\frac{K(\mathbf{r})}{2}\hat{\pi} + v_s(\mathbf{r},t), \tag{43}$$

where

$$\hat{\pi} = \hat{\mathbf{p}} + \mathbf{A}_s(\mathbf{r},t). \tag{44}$$

The scalar-relativistic induced current density within the ZORA can now be obtained from the nonrelativistic current density in Eq. (15) by the substitution of the auxiliary operator $\tilde{\mathbf{j}}_{p,\mathbf{g}}$ by the auxiliary operator

$$\tilde{\mathbf{j}}^{\mathrm{ZORA}}_{p,\mathbf{g}} = \frac{-i}{2}[e^{-i\mathbf{g}\cdot\mathbf{r}}K(\mathbf{r})\,\nabla - \nabla^\dagger K(\mathbf{r})e^{-i\mathbf{g}\cdot\mathbf{r}}] \tag{45}$$

in the response functions given in Eq. (22).

As we will show in the next section, in our implementation we will need the curl of the induced current density,

$$\delta\mathbf{m}(\mathbf{r},\omega) = \nabla \times \delta\mathbf{j}(\mathbf{r},\omega). \tag{46}$$

In a similar way as for $\delta\mathbf{j}$ we can write

$$\delta\mathbf{m}(\mathbf{r},\omega) = e^{i\mathbf{g}\cdot\mathbf{r}}\delta\mathbf{m}_{\mathbf{g}}(\mathbf{r},\omega). \tag{47}$$

An expression for $\delta\mathbf{m}_{\mathbf{g}}(\mathbf{r},\omega)$ can be obtained from Eq. (17) by taking the curl on either side which amounts to the substitution of $\tilde{\mathbf{m}}_{\mathbf{g}} = -i(\nabla^\dagger e^{-i\mathbf{g}\cdot\mathbf{r}} \times \nabla)$ for $\tilde{a}_{\mathbf{g}}$ in the Kohn-Sham response functions given in Eq. (22). In the case that we consider scalar relativistic effects within the ZORA we can do a similar evaluation to obtain the auxiliary operator $\tilde{\mathbf{m}}^{\mathrm{ZORA}}_{\mathbf{g}}$. It is given by

$$\tilde{\mathbf{m}}^{\mathrm{ZORA}}_{\mathbf{g}} = -i[\nabla^\dagger e^{-i\mathbf{g}\cdot\mathbf{r}}K(\mathbf{r}) \times \nabla] - \frac{i}{2}\{e^{-i\mathbf{g}\cdot\mathbf{r}}[\nabla K(\mathbf{r})] \times \nabla + \nabla^\dagger \times [\nabla K(\mathbf{r})]e^{-i\mathbf{g}\cdot\mathbf{r}}\}. \tag{48}$$

For the materials discussed in this paper $K(\mathbf{r}) \approx 1$ and $\nabla v_{s,0}(\mathbf{r}) \ll 2c^2$ everywhere except close to the nuclei. The term $\nabla K(\mathbf{r}) = K^2(\mathbf{r})\nabla v_{s,0}(\mathbf{r})/(2c^2)$ is thus smaller than one everywhere, except in a small volume around the nuclei which, however, has a negligible contribution to the integrals in which it appears. Therefore we will neglect the second term on the right-hand side of Eq. (48).

III. IMPLEMENTATION

As shown in Ref. 13 we can write $\delta\mathbf{A}_{xc}(\mathbf{r},\omega)$ as expressed in Eqs. (28)–(30) in a more convenient way,

$$\delta\mathbf{A}_{xc}(\mathbf{r},\omega) = -\frac{i}{\omega}\nabla[\delta v^{\mathrm{ALDA}}_{xc}(\mathbf{r},\omega) + \delta u_{xc}(\mathbf{r},\omega)] + \delta\mathbf{a}_{xc}(\mathbf{r},\omega) + \nabla \times \delta\mathbf{b}_{xc}(\mathbf{r},\omega), \tag{49}$$

where $\delta u_{xc}(\mathbf{r},\omega)$ is a scalar field, $\delta\mathbf{a}_{xc}(\mathbf{r},\omega)$ is a polar vector field, $\delta\mathbf{b}_{xc}(\mathbf{r},\omega)$ is an axial vector field. These fields can be written in the following compact matrix vector product:[13]

$$\begin{pmatrix} \delta u_{xc} \\ i\omega\delta\mathbf{a}_{xc} \\ i\omega\delta\mathbf{b}_{xc} \end{pmatrix} = \begin{pmatrix} y_{\rho\rho} & y_{\rho\mathbf{j}} & 0 \\ y_{\mathbf{j}\rho} & y_{\mathbf{jj}} & y_{\mathbf{jm}} \\ 0 & y_{\mathbf{mj}} & y_{\mathbf{mm}} \end{pmatrix} \begin{pmatrix} \delta\rho \\ i\delta\mathbf{j}/\omega \\ i\delta\mathbf{m}/\omega \end{pmatrix}. \tag{50}$$

The matrix entries are given as

$$y_{\rho\rho} = -i\omega\frac{\frac{4}{3}\tilde{\eta}_{xc} + \tilde{\zeta}_{xc}}{\rho_0^2}, \tag{51}$$

$$y_{\rho\mathbf{j}} = y^T_{\mathbf{j}\rho} = -i\omega\left(\frac{\frac{4}{3}\tilde{\eta}_{xc} + \tilde{\zeta}_{xc}}{\rho_0^2} - 2\frac{\tilde{\eta}'_{xc}}{\rho_0}\right)\frac{\nabla\rho_0}{\rho_0}, \tag{52}$$

$$y_{\mathbf{jj}} = -i\omega\left(\frac{\frac{1}{3}\tilde{\eta}_{xc} + \tilde{\zeta}_{xc}}{\rho_0^2} - 4\frac{\tilde{\eta}'_{xc}}{\rho_0} + 2\tilde{\eta}''_{xc}\right)\frac{\nabla\rho_0 \otimes \nabla\rho_0}{\rho_0^2} - i\omega\left(2\frac{\tilde{\eta}'_{xc}}{\rho_0}\frac{\nabla \otimes \nabla\rho_0}{\rho_0} + \frac{\tilde{\eta}_{xc}}{\rho_0^2}\frac{|\nabla\rho_0|^2}{\rho_0^2}\mathbf{I}\right), \tag{53}$$

$$y_{\mathbf{jm}} = y^T_{\mathbf{mj}} = -i\omega\frac{\tilde{\eta}_{xc}}{\rho_0^2}\left(\frac{\nabla\rho_0}{\rho_0} \times\right), \tag{54}$$

$$y_{\mathbf{mm}} = -i\omega\frac{\tilde{\eta}_{xc}}{\rho_0^2}\mathbf{I}, \tag{55}$$

in which we define the antisymmetric 3×3 matrix $(\nabla\rho_0/\rho_0 \times)_{ij} = -\Sigma_k \epsilon_{ijk}(\partial_k\rho_0)/\rho_0$ and where $\tilde{\eta}'_{xc}(\mathbf{r},\omega)$ and $\tilde{\eta}''_{xc}(\mathbf{r},\omega)$ are

the first- and second-order derivatives of $\tilde{\eta}_{xc}(\mathbf{r},\omega)$ with respect to the ground-state density. The matrix in Eq. (50) is a local function of the ground-state density and its first- and second-order gradients and has additional ω dependence through the coefficients $\tilde{\eta}_{xc}(\mathbf{r},\omega)$ and $\tilde{\zeta}_{xc}(\mathbf{r},\omega)$.

Using Eq. (49) the exchange-correlation contribution to the perturbation given in Eq. (6) can now be rewritten within our linear response formulation as

$$\delta\hat{H}_{xc}(\mathbf{r},\omega) = \tilde{\rho}_{-\mathbf{g}}[\delta v^{\mathrm{ALDA}}_{\mathbf{g},xc}(\mathbf{r},\omega) + \delta u_{\mathbf{g},xc}(\mathbf{r},\omega)] + \tilde{\mathbf{j}}_{p,-\mathbf{g}} \cdot \delta\mathbf{a}_{\mathbf{g},xc}(\mathbf{r},\omega) + \tilde{\mathbf{m}}_{-\mathbf{g}} \cdot \delta\mathbf{b}_{\mathbf{g},xc}(\mathbf{r},\omega), \tag{56}$$

In the case of Au where we include scalar relativistic effects within the ZORA one should read $\tilde{\mathbf{j}}^{\mathrm{ZORA}}_{p,-\mathbf{g}}$ and $\tilde{\mathbf{m}}^{\mathrm{ZORA}}_{-\mathbf{g}}$ instead of $\tilde{\mathbf{j}}_{p,-\mathbf{g}}$ and $\tilde{\mathbf{m}}_{-\mathbf{g}}$ in Eq. (56). Using Eq. (56) the self-consistent linear-response equations (18) and (19) can be written in the following form:

$$\begin{pmatrix} \delta\rho^{\mathrm{inter}}_{\mathbf{g}} \\ i\delta\mathbf{j}^{\mathrm{inter}}_{\mathbf{g}}/\omega \\ i\delta\mathbf{m}^{\mathrm{inter}}_{\mathbf{g}}/\omega \end{pmatrix} = \begin{pmatrix} \chi^{\mathrm{inter}}_{\rho\rho\mathbf{g}} & -i\chi^{\mathrm{inter}}_{\rho\mathbf{j}_p\mathbf{g}}/\omega & -i\chi^{\mathrm{inter}}_{\rho\mathbf{mg}}/\omega \\ i\chi^{\mathrm{inter}}_{\mathbf{j}_p\rho\mathbf{g}}/\omega & \Delta\chi^{\mathrm{inter}}_{\mathbf{j}_p\mathbf{j}_p\mathbf{g}}/\omega^2 & \Delta\chi^{\mathrm{inter}}_{\mathbf{j}_p\mathbf{mg}}/\omega^2 \\ i\chi^{\mathrm{inter}}_{\mathbf{m}\rho\mathbf{g}}/\omega & \Delta\chi^{\mathrm{inter}}_{\mathbf{mj}_p\mathbf{g}}/\omega^2 & \Delta\chi^{\mathrm{inter}}_{\mathbf{mmg}}/\omega^2 \end{pmatrix} \times \begin{pmatrix} \delta v_{\mathbf{g},H,\mathrm{mic}} + \delta v^{\mathrm{ALDA}}_{\mathbf{g},xc,\mathrm{mic}} + \delta u_{\mathbf{g},xc} \\ i\omega(\delta\mathbf{A}_{\mathbf{g},\mathrm{mac}} + \delta\mathbf{a}_{\mathbf{g},xc}) \\ i\omega\delta\mathbf{b}_{\mathbf{g},xc} \end{pmatrix}, \tag{57}$$

for the interband parts, and as

$$i\omega\begin{pmatrix} \omega/g\,\delta\rho^{\mathrm{intra}}_{\mathbf{g}} \\ \delta\mathbf{j}^{\mathrm{intra}}_{\mathbf{g}} \\ \delta\mathbf{m}^{\mathrm{intra}}_{\mathbf{g}} \end{pmatrix} = \begin{pmatrix} \omega^2/g^2\chi^{\mathrm{intra}}_{\rho\rho\mathbf{g}} & \omega/g\chi^{\mathrm{intra}}_{\rho\mathbf{j}_p\mathbf{g}} & \omega/g\chi^{\mathrm{intra}}_{\rho\mathbf{mg}} \\ \omega/g\chi^{\mathrm{intra}}_{\mathbf{j}_p\rho\mathbf{g}} & \Delta\chi^{\mathrm{intra}}_{\mathbf{j}_p\mathbf{j}_p\mathbf{g}} & \Delta\chi^{\mathrm{intra}}_{\mathbf{j}_p\mathbf{mg}} \\ \omega/g\chi^{\mathrm{intra}}_{\mathbf{m}\rho\mathbf{g}} & \Delta\chi^{\mathrm{intra}}_{\mathbf{mj}_p\mathbf{g}} & \Delta\chi^{\mathrm{intra}}_{\mathbf{mmg}} \end{pmatrix} \times \begin{pmatrix} ig(\delta v_{\mathbf{g}H,\mathrm{mic}} + \delta v^{\mathrm{ALDA}}_{\mathbf{g},xc,\mathrm{mic}} + \delta u_{\mathbf{g},xc}) \\ i\omega(\delta\mathbf{A}_{\mathbf{g},\mathrm{mac}} + \delta\mathbf{a}_{\mathbf{g},xc}) \\ i\omega\delta\mathbf{b}_{\mathbf{g},xc} \end{pmatrix}, \tag{58}$$

for the intraband contributions, with $\Delta\chi_{\mathbf{abg}} = [\chi_{\mathbf{abg}}(\omega) - \chi_{\mathbf{abg}}(\omega=0)]$. The matrix vector products in the above expressions again include an integration over a real-space coordinate. The above relations have been written in such a way that all matrix elements are real and finite in the limit $(\mathbf{g},\omega)\to(0,0)$. The explicit expressions for the Kohn-Sham response functions have been given in Refs. 3 and 13. In the limit of vanishing $\mathbf{g}$ the set of equations (57) reduces to that one used in the case of nonmetallic crystalline systems[13] for which we need to consider only fully occupied bands and fully unoccupied bands. In this limit the term $ig(\delta v_{\mathbf{g}H,\mathrm{mic}} + \delta v^{\mathrm{ALDA}}_{\mathbf{g},xc,\mathrm{mic}} + \delta u_{\mathbf{g},xc})$ on the right-hand side of Eqs (58) vanishes.[3] Therefore in the optical limit $\mathbf{g}\to 0$ the intraband parts of the density, the current density and the curl of current density only have contributions from the macroscopic vector potential and the terms $\delta\mathbf{a}_{\mathbf{g},xc}$ and $\delta\mathbf{b}_{\mathbf{g},xc}$ that enter the VK expression for the exchange-correlation vector potential. Once the two sets of Eqs. (57) and (58) are solved we can calculate the macroscopic dielectric function as

$$\epsilon(\omega) = 1 + 4\pi\chi_e(\omega), \tag{59}$$

where $\chi_e(\omega)$ is the electric susceptibility, and the electron energy loss function as

$$\frac{2\pi}{k^2V}S(\mathbf{g},\omega) = -\,\mathrm{Im}\,\frac{1}{\hat{\mathbf{g}}\cdot\epsilon(\mathbf{g},\omega)\cdot\hat{\mathbf{g}}}, \tag{60}$$

where $S(\mathbf{g},\omega)$ is the dynamical structure factor. The above expression is valid for general $\mathbf{g}$. Here we evaluate it in the optical limit $\mathbf{g}\to 0$. In a recent work[3] it was shown that within the ALDA the intraband contribution to the dielectric function is real when evaluated in the optical limit. Therefore there is no intraband contribution to the absorption spectrum within this approximation. By using the Vignale-Kohn functional it is no longer possible to separate interband and intraband contributions to the dielectric function. Interband and intraband processes are coupled through the exchange-correlation potentials $\delta\mathbf{a}_{\mathbf{g},xc}$ and $\delta\mathbf{b}_{\mathbf{g},xc}$ which are complex vectors, and give rise to the Drude-like tail on the low-frequency range of the absorption spectrum.

IV. RESULTS

We calculated the macroscopic dielectric functions $\epsilon(\omega)$ and the electron energy loss functions $-\mathrm{Im}[\epsilon(\omega)]^{-1}$ in the spectral range 0–10 eV for the isotropic crystals of copper, silver, and gold in a fcc lattice. We used the experimental lattice constants 3.61 Å for Cu, 4.09 Å for Ag, and 4.08 Å for Au. All calculations were performed using a modified version of the ADF-BAND program.[1–3,50–52] We made use of a hybrid valence basis set consisting of Slater-type orbitals (STOs) in combination with the numerical solutions of a free-atom Herman-Skillman program.[53] Cores were kept frozen up to $3p$ for Cu, $4p$ for Ag, and $4f$ for Au. The spatial resolution of this basis is equivalent to a STO triple-zeta basis set augmented with two polarization functions.[54] The Herman-Skillman program also provides us with the free-atom Kohn-Sham potential. The crystal potential was evaluated using an auxiliary basis set of STO functions to fit the deformation density in the ground-state calculation and the induced density in the response calculation. For the evaluation of the $\mathbf{k}$-space integrals we used a numerical integration scheme with 175 symmetry-unique sample points in the irreducible wedge of the Brillouin zone, which was constructed by adopting a Lehmann-Taut tetrahedron scheme.[55,56] In all our ground-state calculations we used the local density approximation (LDA) for the exchange-correlation functional. In the response calculations we employed the Vignale-Kohn functional. All results shown here were obtained using the Vosko-Wilk-Nusair parametrization[10] of the LDA exchange-correlation potential, which was also used to derive the ALDA exchange-correlation kernel, and both the QVA and CNT parametrizations for the longitudinal and transverse kernels $f^{h}_{xcL,T}(\omega)$ which enter the VK expression for the exchange-correlation vector potential. In Figs. 1–3 the real and imaginary parts of the dielectric functions of Cu, Ag, and Au are reported. The results obtained using the VK func-

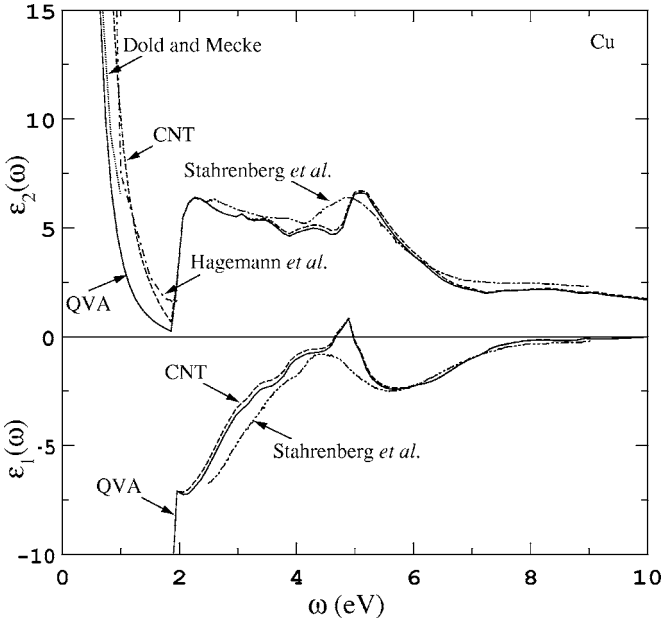

FIG. 1. The calculated and measured real $[\epsilon_1(\omega)]$ and imaginary $[\epsilon_2(\omega)]$ parts of the dielectric function of copper. The calculated spectra were obtained using the VK functional with both the QVA and CNT parametrizations for the exchange-correlation kernels of the homogeneous electron gas. The experimental results are taken from Refs. 16–18.

tional with the QVA and CNT parametrizations $f^h_{xcL,T}(\omega)$ are in close agreement. The main difference is the Drude-like tail in the absorption spectra where the two results are roughly 0.25 eV apart. For convenience we do not report the ALDA

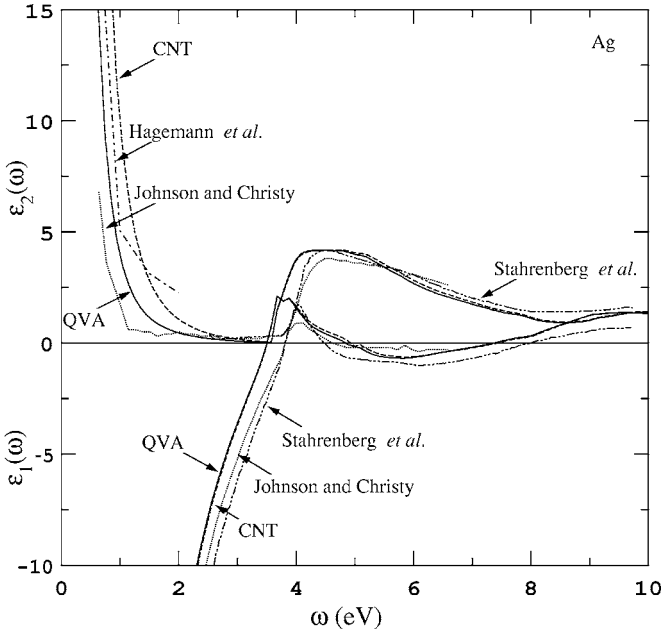

FIG. 2. The calculated and measured real $[\epsilon_1(\omega)]$ and imaginary $[\epsilon_2(\omega)]$ parts of the dielectric function of silver. The calculated spectra were obtained using the VK functional with both the QVA and CNT parametrizations for the exchange-correlation kernels of the homogeneous electron gas. The experimental results are taken from Refs. 16, 18, and 19.

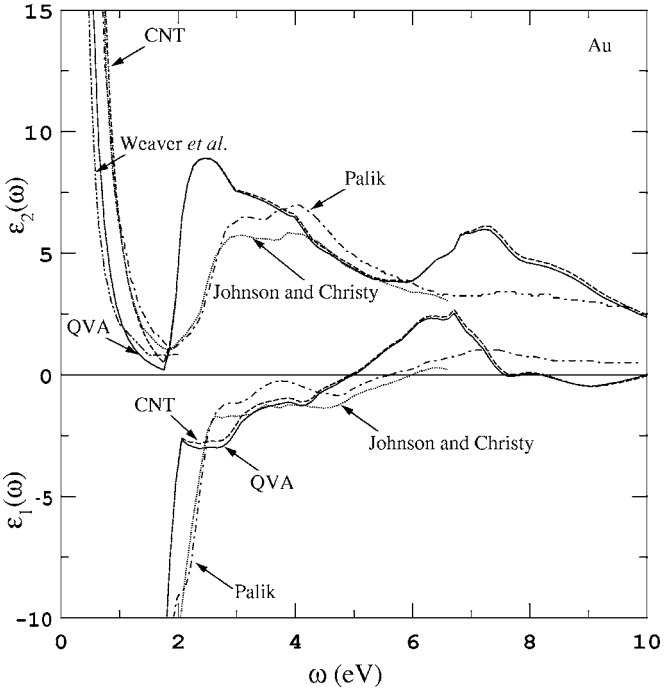

FIG. 3. The calculated and measured real $[\epsilon_1(\omega)]$ and imaginary $[\epsilon_2(\omega)]$ parts of the dielectric functions of gold. The calculated spectra were obtained using the VK functional with both the QVA and CNT parametrizations for the exchange-correlation kernels of the homogeneous electron gas. The experimental results are taken from Refs. 19–21. The theoretical curves are results of scalar-relativistic calculations.

results[3,57] since they are almost identical to the VK results with the important exception that the Drude-like tail in its absorption spectrum is absent since the ALDA is a local function in time and therefore cannot describe relaxation processes. When the VK functional is employed we obtain a Drude-like tail in the low-frequency range. This absorption is due to relaxation processes of which the part due to electron-electron scattering can be described by using an exchange-correlation functional that is nonlocal in time. In the appendix we analyze the low-frequency behavior of the dielectric function within our method. There we show that in the case we apply the Vignale-Kohn functional with $\mu_{xc}=0$, for frequencies bigger than a characteristic frequency ω_1, which we defined in the appendix, the real part of the dielectric function diverges as ω^{-2}, whereas the imaginary part should decay as ω^{-3}. For frequencies below ω_1, the real part of the dielectric function is finite whereas the imaginary part diverges as ω^{-1}. If on the other hand we apply the Vignale-Kohn functional with $\mu_{xc}\neq 0$ we obtain the same low-frequency behavior as we found above for the case $\mu_{xc}=0$ with the important difference that for frequencies below a characteristic frequency $\omega_0<\omega_1$, which we defined in the appendix, the imaginary part of the dielectric function will go to zero as ω. Therefore, instead of a Drude-like tail we observe a low-frequency peak in our calculated absorption spectra around ω_1.

The low-frequency behavior we obtain with the Vignale-Kohn functional with $\mu_{xc}=0$ is in agreement with the de-

scription of the intraband contribution to the dielectric function within the classical Drude model. Within this simple model the real and imaginary parts of the dielectric functions, $\epsilon_1(\omega)$ and $\epsilon_2(\omega)$, respectively, are given by

$$\epsilon_1^D(\omega) = 1 - \frac{\omega_p^2 \tau^2}{1 + \omega^2 \tau^2}, \tag{61}$$

$$\epsilon_2^D(\omega) = \frac{\omega_p^2 \tau}{\omega(1 + \omega^2 \tau^2)}, \tag{62}$$

with ω_p the plasma frequency and the τ the relaxation time. The latter is in general frequency dependent.[58–61] For $\omega\tau \gg 1$, which is true for the near infrared, Eqs. (61) and (62) become

$$\epsilon_1^D(\omega) = 1 - \frac{\omega_p^2}{\omega^2}, \tag{63}$$

$$\epsilon_2^D(\omega) = \frac{\omega_p^2}{\omega^3 \tau}. \tag{64}$$

The real part of the dielectric function scales as ω^{-2}, whereas the imaginary part scales as ω^{-3} for a frequency-independent τ, in agreement with our calculations. For $\omega\tau \ll 1$, the Drude equations reduce to

$$\epsilon_1^D(\omega) = 1 - \omega_p^2 \tau^2, \tag{65}$$

$$\epsilon_2^D(\omega) = \frac{\omega_p^2 \tau}{\omega}. \tag{66}$$

Again we find a qualitative agreement between the Drude description and our model: a finite real part and an imaginary part which scales as ω^{-1}. We note that in our calculations we only take into account relaxation processes due to electron-electron scattering whereas the Drude model also describes relaxation processes due to other phenomena such as electron-phonon scattering. Our results are in good agreement with the experimental results although the spectra obtained for gold show some discrepancies, especially the first peak in the absorption spectrum is not well described. The Drude-like tails in the absorption spectra seem to be well described for the three materials. However, since we only consider relaxation processes due to electron-electron scattering and not those due to electron-phonon scattering our results should be below those obtained with experiment. Therefore the QVA parametrization used in the VK functional performs better than the CNT parametrization, since the results we obtain for the Drude-like tails using the former do not overestimate the experimental Drude-like tails. Our results are also in agreement with accurate results obtained from solving the Bethe-Salpeter equation (BSE).[23] In particular, the Drude-like tails in these BSE spectra are close to the experimental tails indicating that indeed the electron-electron contribution to the scattering is dominant in the frequency range that we consider. In Fig. 4 we show the electron energy loss spectra (EELS) of Cu, Ag, and Au. The EELS of Cu and Au are already well-described within the ALDA.[3] Again the results obtained using the VK functional

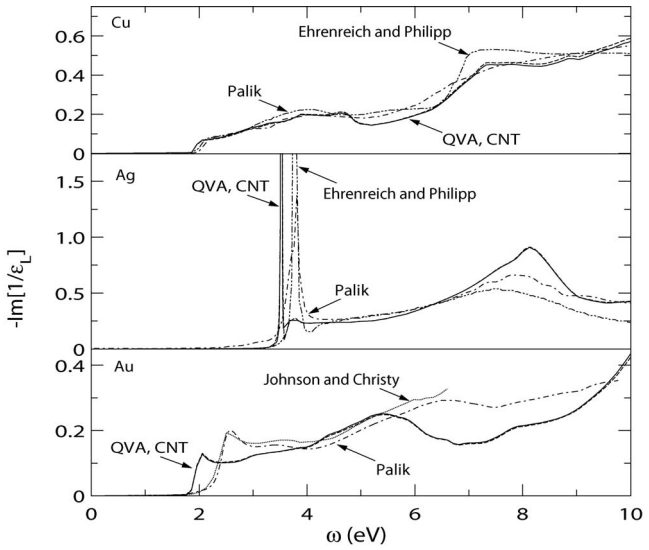

FIG. 4. The calculated and measured electron-energy loss spectra of copper, silver, and gold. The experimental results are taken from Refs. 15, 19, and 20. The calculated results reported for Au refer to scalar-relativistic calculations. Since the QVA and CNT spectra are very close to each other we only use one arrow in each panel to indicate both spectra. The QVA spectra and the CNT spectra are denoted by the continuous and dashed curve, respectively.

with the two parametrizations are in close agreement with each other and with the results obtained within the ALDA. The ALDA fails to reproduce the finite width of the sharp plasmon peak at about 3.8 eV in the EELS of silver.[15,20] In the EELS obtained with the VK functional one obtains a plasmon peak with finite width. The appearance of this peak is due to the fact that now the imaginary part of the dielectric function is small but nonvanishing at the frequency where the real part crosses the zero axis. This feature is qualitatively well described by the VK functional with the QVA and CNT parametrizations for $f_{xcL,T}^h(\omega)$, although its position is redshifted by about 0.3 eV with respect to the experiments as a direct consequence of the underestimation of the onset energy of the interband absorption. Furthermore, the height of the plasmon peak in our calculations is larger than that in the reported experiments. The heights of the QVA and CNT peaks are 10.5 and 8.2, respectively, whereas the heights of the peaks reported by Palik and by Ehrenreich and Philipp are about 1.4 and 3.9, respectively.[15,20] However, these experiments were performed at room temperature. Morgan and Lynch showed that the height of this plasmon resonance increases significantly when the temperature is decreased.[22] At room temperature they obtain a plasmon peak with a height of about 3.0, whereas at 4.4 K they obtain a peak of about 4.8. They also showed that the level of impurities in the sample strongly influences the height of the peak, which decreases with increasing impurity level. Therefore the experimental results can be considered a lower bound for the results obtained from calculations on perfect crystals at zero temperature. We can thus consider our results to give a reasonable estimation of the height of the plasmon peak. This plasmon peak has been calculated by Marini *et al.* as well within the GW approximation.[24] They obtain a good agree-

ment with the measurements performed by Palik.[20]

V. CONCLUSIONS

In this paper we have included the Vignale-Kohn expression for the exchange-correlation vector potential in our formulation of the linear response of metals within the time-dependent current-density approach. This functional is nonlocal in time and therefore relaxation effects due to electron-electron scattering could be taken into account. The evaluation of the VK functional requires the knowledge of the exchange-correlation kernels of the homogeneous electron gas $f^h_{xcL,T}(\omega)$ as a function of the density and the frequency. We have used the two existing parametrizations for $f^h_{xcL,T}(\omega)$ by Conti, Nifosì, and Tosi and by Qian and Vignale. In the optical limit $\mathbf{g}\to 0$ the two sets of self-consistent equations describing the interband and intraband contributions to the response remain coupled when the Vignale-Kohn expression for the exchange-correlation vector potential is included. We have calculated the dielectric and electron energy loss functions of copper, silver, and gold and we have compared them with the best available measurements reported in literature and with our results from calculations within the adiabatic local density approximation. The VK functional yields results which are in good agreement with the experimental results and BSE results. The real parts of the dielectric functions and the regions in the absorption spectra where the interband processes are dominant are similarly described by the two approximations and are close to previous results obtained within the ALDA. In addition, the VK functional reproduces the low-frequency Drude-like tails in the absorption spectra, which were absent in the previous ALDA calculations. The electron energy loss spectra obtained with the VK functional are close to the spectra obtained within the ALDA with a notable difference in the case of silver: the first sharp plasmon peak found in the experimental EELS is well described in the spectrum obtained with the VK functional with a finite width contrary to the ALDA spectrum. Therefore, the VK functional with μ_{xc} set to zero provides an efficient way to obtain results for the optical spectra and EELS of metals that are comparable to BSE results. Our results are, however, obtained at much lower computational cost. Furthermore, we gave justifications of our choice to set μ_{xc} equal to zero.

APPENDIX: LOW-FREQUENCY BEHAVIOR OF THE DIELECTRIC FUNCTION

We define two vectors $\mathbf{P}$ and $\mathbf{F}$ as

$$\mathbf{P}=\begin{pmatrix}\delta\rho\\ i\delta\mathbf{j}/\omega\\ i\delta\mathbf{m}/\omega\end{pmatrix}, \tag{A1}$$

containing the densities, in which the interband and intraband contributions are added, i.e., $\delta\rho=\delta\rho^{\text{inter}}+\delta\rho^{\text{intra}}$ and similarly for $\delta\mathbf{j}$ and $\delta\mathbf{m}$, and

$$\mathbf{F}=\begin{pmatrix}0\\ i\omega\delta\mathbf{A}_{\text{mac}}\\ 0\end{pmatrix}+\begin{pmatrix}\delta v^{\text{ALDA}}_{Hxc,\text{mic}}\\ 0\\ 0\end{pmatrix}+\begin{pmatrix}\delta u_{xc}\\ i\omega\delta\mathbf{a}_{xc}\\ i\omega\delta\mathbf{b}_{xc}\end{pmatrix}, \tag{A2}$$

which contains all first-order contributions to the perturbing potentials. Here the perturbation $\mathbf{F}$ is decomposed into three terms: $\mathbf{F}_{\text{mac}}$ containing only the macroscopic field, $\mathbf{F}_a$ containing the adiabatic parts given by the microscopic Hartree potential and the ALDA exchange-correlation potential $\delta v^{\text{ALDA}}_{Hxc,\text{mic}}=\delta v_{H,\text{mic}}+\delta v^{\text{ALDA}}_{xc,\text{mic}}$, and $\mathbf{F}_d$ containing the dynamic part of the exchange-correlation vector potential. From Eqs. (57) and (58) it becomes clear that we can write

$$\mathbf{P}=\left(X^{\text{inter}}+\frac{1}{\omega^2}Q^{\dagger}X^{\text{intra}}\cdot Q\right)\cdot\mathbf{F}, \tag{A3}$$

where

$$Q=\begin{pmatrix}ig & 0 & 0\\ 0 & 1 & 0\\ 0 & 0 & 1\end{pmatrix}, \tag{A4}$$

and X^{inter} and X^{intra} are the matrices of the interband and intraband Kohn-Sham response functions given in Eqs. (57) and (58). In the linear response regime we can write $\mathbf{F}_a=Y_a\cdot\mathbf{P}$ for the adiabatic part of the potential vector, and $\mathbf{F}_d=Y_d\cdot\mathbf{P}$ for the dynamic part. Here the matrix Y_d is the matrix that enters Eq. (50) and Y_a is defined as

$$Y_a=\begin{pmatrix}y_a & 0 & 0\\ 0 & 0 & 0\\ 0 & 0 & 0\end{pmatrix}, \tag{A5}$$

with the frequency independent kernel y_a defined by the relation $y_a\delta\rho=\delta v^{\text{ALDA}}_{Hxc,\text{mic}}$. The total perturbing potential is then given by

$$\mathbf{F}=\mathbf{F}_{\text{mac}}+(Y_a+Y_d)\cdot\mathbf{P}. \tag{A6}$$

The low-frequency behavior of the matrix Y_d is determined by the low-frequency behavior of the viscoelastic coefficients $\tilde{\eta}_{xc}(\mathbf{r},\omega)$ and $\tilde{\zeta}_{xc}(\mathbf{r},\omega)$ which in turn is determined by the low-frequency behavior of $f_{xcL,T}(\omega)$. Since $f_{xcL,T}(\omega)=f^*_{xcL,T}(-\omega)$ and considering the results obtained in Eqs. (37) and (38) we can write the following expressions for the low-frequency behavior of $\tilde{\eta}_{xc}(\mathbf{r},\omega)$ and $\tilde{\zeta}_{xc}(\mathbf{r},\omega)$:

$$\frac{-i\omega\tilde{\zeta}_{xc}}{\rho_0^2(\mathbf{r})}=i\omega A+\omega^2 B+O(\omega^3), \tag{A7}$$

$$\frac{-i\omega\tilde{\eta}_{xc}}{\rho_0^2(\mathbf{r})}=\frac{\mu_{xc}}{\rho_0^2(\mathbf{r})}+i\omega C+\omega^2 D+O(\omega^3), \tag{A8}$$

where A, B, C, and D are real. Furthermore, from the work of Qian and Vignale[12] we know the exact result for the slope of the imaginary parts of $f^h_{xcL,T}(\omega)$ in the limit $\omega\to 0$, which they show to be finite. This means that in the above expressions A and C are finite. Using Eqs. (A7) and (A8), we can write the following low-frequency expansion for Y_d:

$$Y_d = \sum_p (i\omega)^p Y_{d,p}, \tag{A9}$$

where all $Y_{d,p}$ are real and $Y_{d,0} \propto \mu_{xc}$. It now becomes clear that we can obtain $\mathbf{P}$ by solving Eqs. (A3) and (A6) self-consistently. We have carefully formulated these response equations such that a regular solution can be found for $\lim_{\mathbf{g}\to 0} \mathbf{P}(\mathbf{g}) = \mathbf{P}$, with $\mathbf{P}$ the solution of Eq. (A3) at $\mathbf{g}=\mathbf{0}$. In this limit we can write the following low-frequency expression of Eq. (A3):

$$\left[\omega^2 I - \left(\omega^2 \sum_p (i\omega)^p X_p^{\text{inter}} + \tilde{X}^{\text{intra}}\right)\left(Y_a + \sum_p (i\omega)^p Y_{d,p}\right)\right] \cdot \mathbf{P} = \left(\omega^2 \sum_p (i\omega)^p X_p^{\text{inter}} + \tilde{X}^{\text{intra}}\right) \cdot \mathbf{F}_{\text{mac}}, \tag{A10}$$

where, since $X^{\text{inter}}(\omega) = X^{\text{inter}*}(-\omega)$, we have used the series expansion $X^{\text{inter}} = \Sigma_p (i\omega)^p X_p^{\text{inter}}$. Here the matrices X_{2p+1}^{inter} vanish if ω is below the interband absorption edge, and the matrix $\tilde{X}^{\text{intra}}$ is frequency independent and defined as

$$\tilde{X}^{\text{intra}} = \lim_{\mathbf{g}\to 0} Q^\dagger \cdot X^{\text{intra}} \cdot Q = \begin{pmatrix} 0 & 0 & 0 \\ 0 & \Delta\chi^{\text{intra}}_{\mathbf{j}_p\mathbf{j}_p} & \Delta\chi^{\text{intra}}_{\mathbf{j}_p\mathbf{m}} \\ 0 & \Delta\chi^{\text{intra}}_{\mathbf{m}\mathbf{j}_p} & \Delta\chi^{\text{intra}}_{\mathbf{m}\mathbf{m}} \end{pmatrix}. \tag{A11}$$

All matrices are real valued. Note that due to their matrix structure the product $\tilde{X}^{\text{intra}} Y_a$ vanishes. From Eq. (A10) it immediately becomes clear that the low frequency behavior of the solution is largely determined by $\tilde{X}^{\text{intra}}$ and the low frequency coefficients of Y_d. Since $\mathbf{P}(\omega) = \mathbf{P}^*(-\omega)$, we can use the series expansion $\mathbf{P} = \Sigma_{n=n_0}^{\infty} (i\omega)^n \mathbf{P}_n$, where we assume that the expansion truncates at a certain value n_0 since we are interested in the low-frequency behavior of $\mathbf{P}$. We can then write Eq. (A10) as

$$\left(\sum_{p=0}^{\infty} (i\omega)^p X_p\right)\left(\sum_{n=n_0}^{\infty} (i\omega)^n \mathbf{P}_n\right) = \sum_{m=0}^{\infty} (i\omega)^m \mathbf{F}_m, \tag{A12}$$

with

$$X_p = -\delta_{p,2} I + X_{p-2}^{\text{inter}} Y_a - \tilde{X}^{\text{intra}} Y_{d,p} + \sum_{s=0}^{p-2} X_{p-s-2}^{\text{inter}} Y_{d,s}, \tag{A13}$$

$$\mathbf{F}_m = (-X_{m-2}^{\text{inter}} + \delta_{m,0} \tilde{X}^{\text{intra}}) \mathbf{F}_{\text{mac}}. \tag{A14}$$

Note that the odd-indexed potential coefficients vanish, $\mathbf{F}_{2m+1} = \mathbf{0}$. We mention the first two matrix and vector elements in particular,

$$X_0 = -\tilde{X}^{\text{intra}} Y_{d,0}, \quad \mathbf{F}_0 = \tilde{X}^{\text{intra}} \mathbf{F}_{\text{mac}}, \tag{A15}$$

$$X_1 = -\tilde{X}^{\text{intra}} Y_{d,1}, \quad \mathbf{F}_1 = \mathbf{0}. \tag{A16}$$

By equating all orders in Eq. (A12) separately, we obtain the general structure of the mth order of the low-frequency expansion of the response equation, which is given by the relation

$$\sum_{n=n_0}^{m} X_{m-n} \mathbf{P}_n = \mathbf{F}_m \tag{A17}$$

with $\mathbf{F}_{m<m_0} = \mathbf{0}$, in which we need to choose $n_0 \leqslant m_0$ such that there is a unique solution. The dimension of the matrices and vectors is d. This infinite set of equations can be written in the following triangular block matrix form:

$$\begin{bmatrix} X_0 & 0 & 0 & \cdots \\ X_1 & X_0 & 0 & \ddots \\ X_2 & X_1 & X_0 & \ddots \\ \vdots & \ddots & \ddots & \ddots \end{bmatrix} \begin{bmatrix} \mathbf{P}_{n_0} \\ \vdots \\ \mathbf{P}_{m_0-1} \\ \mathbf{P}_{m_0} \\ \vdots \end{bmatrix} = \begin{bmatrix} \mathbf{0} \\ \vdots \\ \mathbf{0} \\ \mathbf{F}_{m_0} \\ \vdots \end{bmatrix},$$

from which it becomes clear that there is a unique solution if X_0 is invertible, with $n_0 = m_0$ and $\mathbf{P}_{n<n_0} = 0$, generated by

$$\mathbf{P}_n = X_0^{-1}\left(\mathbf{F}_n - \sum_{m=m_0}^{n-1} X_{n-m} P_m\right).$$

If on the other hand, X_0 is singular as in our case, we proceed to find a solution by constructing the singular value decomposition $X_0 = VDU^\dagger$ with the diagonal matrix D containing singular values $d_1 \cdots d_s = 0$ and $d_{i>s} \neq 0$ with $s > 0$, and the unitary matrices U and V build from the right and left singular vectors spanning the domain, null space and range of X_0. We can multiply each line from the left by $V^\dagger$, and thus remove the first s rows from each diagonal block of the triangular matrix. These rows become replaced by the first s rows of the line below yielding again a triangular form.

$$\begin{bmatrix} \begin{bmatrix} 0 \\ \tilde{D}U^\dagger \end{bmatrix} & 0 & 0 & \cdots \\ V^\dagger X_1 & \begin{bmatrix} 0 \\ \tilde{D}U^\dagger \end{bmatrix} & 0 & \ddots \\ V^\dagger X_2 & V^\dagger X_1 & \begin{bmatrix} 0 \\ \tilde{D}U^\dagger \end{bmatrix} & \ddots \\ \vdots & \ddots & \ddots & \ddots \end{bmatrix} \begin{bmatrix} \mathbf{P}_{n_0} \\ \vdots \\ \mathbf{P}_{m_0-1} \\ \mathbf{P}_{m_0} \\ \vdots \end{bmatrix} = \begin{bmatrix} \mathbf{0} \\ \vdots \\ \mathbf{0} \\ V^\dagger \mathbf{F}_{m_0} \\ \vdots \end{bmatrix}.$$

Here $\tilde{D}$ is the matrix D with the first s rows removed. The first s lines of the equation can be removed as these are trivially satisfied. We can do this by defining new blocks,

$$[X'_n]_{i,j} = \begin{cases} [V^\dagger X_n]_{i+s,j}, & i \leqslant d-s, \\ [V^\dagger X_{n+1}]_{i+s-d,j}, & i > d-s \end{cases} \tag{A18}$$

and similarly new vectors

$$[\mathbf{F}'_n]_i = \begin{cases} [V^\dagger \mathbf{F}_n]_{i+s}, & i \leqslant d-s, \\ [V^\dagger \mathbf{F}_{n+1}]_{i+s-d}, & i > d-s \end{cases} \tag{A19}$$

such that we retrieve the original structure, however, in general, with a nonzero vector $\mathbf{F}'_{m_0-1}$. Therefore we must set $m'_0 = m_0 - 1$. If $\mathbf{F}_{m_0}$ is in the range of X_0 then $\mathbf{F}'_{m_0-1}$ will still be

zero and we can set $m_0'=m_0$. By iterating this procedure k times, until we have found a diagonal block $X_0^{\prime\cdots\prime}$ that is invertible, we have constructed a unique solution that truncates from below at $n_0 \geqslant m_0-k$ with $\mathbf{P}_{n<n_0}=\mathbf{0}$.

We will now discuss three separate cases, being the adiabatic approximation, in which Y_d is set to zero, the dynamic exchange-correlation case with vanishing static limit and hence $Y_{d,0}=0$, but $Y_{d,1}\neq 0$, and the dynamic case with finite static value $Y_{d,0}\neq 0$. In the simplest case (the adiabatic approximation) we have $X_0=X_1=X_{2n+1}=0$, and $\mathbf{F}_{2n+1}=\mathbf{0}$. From Eq. (A17) it immediately follows that in this case the equations for even and odd indexed $\mathbf{P}$ decouple, with the partial result $\mathbf{P}_{2n+1}=\mathbf{0}$. The singular value decompositions for the first two iterations become trivial, $V=U=I$ and $D=0$, and we obtain $n_0=-2$ with the unique even-indexed solutions given by

$$\mathbf{P}_{2n} = X_2^{-1}\left(\mathbf{F}_{2n+2} - \sum_{m=-1}^{n-1} X_{2(n-m+1)}P_{2m}\right), \tag{A20}$$

where we assumed that X_2 is invertible. The susceptibility is therefore purely real valued and is diverging like ω^{-2}. In the dynamic case with vanishing static limit for Y_d, we have $X_0=0$, X_1 singular, $\mathbf{F}_0\neq\mathbf{0}$ but in the range of X_1 (provided that $Y_{d,1}$ is invertible) and again $\mathbf{F}_{2n+1}=\mathbf{0}$. The first iteration is again trivial, with $V=U=I$ and $D=0$. In the second iteration we can remove the singularity of the new diagonal block $X_0'=X_1$, by appying the SVD again. However, if indeed $\mathbf{F}_{-1}'=\mathbf{F}_0$ is in the range of X_1 (which is the case if $Y_{d,1}$ is invertible), then we do not have to decrease m_0 further and we obtain $n_0=-1$, otherwise we do, and find $n_0=-2$. Assuming that the second iteration yields an invertible diagonal block, we have found the solution which truncates at $n_0=-1(-2)$. We can thus conclude that the susceptibility acquires an imaginary part that diverges like ω^{-1}, and a real value that is finite, unless the first-order dynamic exchange-correlation kernel $Y_{d,1}$ is singular. In the dynamic case with finite static limit an extra complication arises. In the first iteration the multiplication from the left with $V^\dagger$ reduces not only the diagonal blocks X_0, but removes also rows from the subdiagonal blocks. This is due to the fact that $X_{0(1)}$ is of the form $\tilde{X}^{\text{intra}}Y_{d,0(1)}$ in which $\tilde{X}^{\text{intra}}$ is singular as is clear from its matrix structure. If the ranges of X_0 and X_1 coincide (which is the case if $Y_{d,0(1)}$ is invertible), then an equal amount of rows is removed in the diagonal and subdiagonal blocks, and also in the vector $\mathbf{F}_0$ if $Y_{d,0(1)}$ is invertible. As always $\mathbf{F}_{2n+1}=\mathbf{0}$. One can check readily that in both iterations we do not need to decrease m_0, and we find a solution with $n_0=0$, assuming that after the second step an invertible diagonal block is generated. In this case the susceptibility is real and finite in the low frequency range. If on the other hand (one of) the matrices $Y_{d,0(1)}$ is singular a divergent ω dependence may still result.

The analysis given above forms the basis for understanding the solution at finite frequency. Retaining only the lowest order terms of the interband response function in Eq. (A10) it becomes clear that we can consider the contribution of $Y_{d,0(1)}$ as small perturbations if $\omega \gg \omega_{0(1)}$, where

$$\omega_0 = \sqrt{\|X_2^{-1}X_0\|}, \tag{A21}$$

$$\omega_1 = \|X_2^{-1}X_1\|, \tag{A22}$$

are two characteristic frequencies defined in terms of the X matrices given in Eq. (A13). Here $\|A\|=\max_i|\lambda_i|$ indicates the spectral norm of the matrix A, being equal to its largest eigenvalue. Including the first-order correction to the adiabatic solution gives

$$\mathbf{P} \approx \left(-\frac{1}{\omega^2}X_2^{-1} - \frac{1}{\omega^4}X_2^{-1}(i\omega X_1 + X_0)X_2^{-1}\right)(\omega^2 X^{\text{inter}} + \tilde{X}^{\text{intra}})\mathbf{F}_{\text{mac}} \tag{A23}$$

and leads to an imaginary part for the susceptibility that decays like $1/\omega^3$ for $\omega<\omega_p$ as then $\omega^2\|X^{\text{inter}}\|<\|\tilde{X}^{\text{intro}}\|$, where it is understood that we consider the frequency range below the optical gap. For $\omega \lesssim \omega_{0(1)}$ the contributions of $Y_{d,0(1)}$ become dominant and determine the solutions as in the analysis given above. Going from high to low frequency we expect a transition from the adiabatic to the dynamic case at around $\max(\omega_0,\omega_1)$, and if $\omega_0<\omega_1$ from the dynamic behavior with vanishing static limit to the case with finite static limit at around ω_0. The results of this analysis are summarized in the following:

$$\chi_e(\omega) \propto \begin{cases} \alpha_1 + i\omega\beta_2, & \omega < \omega_0, \\ \alpha_1' + i\beta_2'/\omega, & \omega_0 < \omega < \omega_1, \\ \alpha_1''/\omega^2 + i\beta_2''/\omega^3, & \omega > \omega_0, \omega_1. \end{cases} \tag{A24}$$

As a special case we have $\omega_0=0$ if $\mu_{xc}=0$.

[1] F. Kootstra, P. L. de Boeij, and J. G. Snijders, J. Chem. Phys. **112**, 6517 (2000).

[2] F. Kootstra, P. L. de Boeij, and J. G. Snijders, Phys. Rev. B **62**, 7071 (2000).

[3] P. Romaniello and P. L. de Boeij, Phys. Rev. B **71**, 155108 (2005).

[4] P. Nozières and D. Pines, *The Theory of Quantum Liquids* (Perseus, Cambridge, MA, 1999).

[5] T. Kreibich and E. K. U. Gross, Phys. Rev. Lett. **86**, 2984 (2001).

[6] R. van Leeuwen, Phys. Rev. B **69**, 115110 (2004).

[7] G. Vignale and W. Kohn, Phys. Rev. Lett. **77**, 2037 (1996).

[8] G. Vignale and W. Kohn, in *Electronic Density Functional Theory: Recent Progress and New Directions*, edited by Dobson *et al.* (Plenum, New York, 1998).

[9] D. M. Ceperley and B. J. Alder, Phys. Rev. Lett. **45**, 566 (1980).

[10] S. H. Vosko, L. Wilk, and M. Nusair, Can. J. Phys. **58**, 1200

(1980).
[11] S. Conti, R. Nifosì, and M. P. Tosi, J. Phys.: Condens. Matter **9**, L475 (1997).
[12] Z. Qian and G. Vignale, Phys. Rev. B **65**, 235121 (2002).
[13] J. A. Berger, P. L. de Boeij, and R. van Leeuwen, Phys. Rev. B **71**, 155104 (2005).
[14] J. A. Berger, P. L. de Boeij, and R. van Leeuwen (unpublished).
[15] H. Ehrenreich and H. R. Philipp, Phys. Rev. **128**, 1622 (1962).
[16] H. J. Hagemann, W. Gudat, and C. Kunz, J. Opt. Soc. Am. **65**, 742 (1975).
[17] B. Dold and R. Mecke, Optik **22**, 435 (1965).
[18] K. Stahrenberg, Th. Herrmann, K. Wilmers, N. Esser, W. Richter, and M. J. G. Lee, Phys. Rev. B **64**, 115111 (2001).
[19] P. B. Johnson and R. W. Christy, Phys. Rev. B **6**, 4370 (1972).
[20] E. D. Palik, *Handbook of Optical Constants of Solids* (Academic, New York, 1985), Vol. I; *ibid.* (Academic, New York, 1991), Vol. II.
[21] J. H. Weaver, C. Krafka, D. W. Lynch, and E. E. Koch, *Optical Properties of Metals* (Physics Data, Fachinformationszentrum, Karlsruhe, 1981).
[22] R. M. Morgan and D. W. Lynch, Phys. Rev. **172**, 628 (1968).
[23] A. Marini and R. Del Sole, Phys. Rev. Lett. **91**, 176402 (2003).
[24] A. Marini, R. Del Sole, and Giovanni Onida, Phys. Rev. B **66**, 115101 (2002).
[25] E. Runge and E. K. U. Gross, Phys. Rev. Lett. **52**, 997 (1984).
[26] A. K. Dhara and S. K. Ghosh, Phys. Rev. A **35**, 442 (1987).
[27] S. K. Ghosh and A. K. Dhara, Phys. Rev. A **38**, 1149 (1988).
[28] E. K. U. Gross, J. F. Dobson, and M. Petersilka, Top. Curr. Chem. **181**, 81 (1996).
[29] G. Vignale, Phys. Rev. B **70**, 201102(R) (2004).
[30] W. Kohn and L. J. Sham, Phys. Rev. **140**, A1133 (1965).
[31] P. Hohenberg and W. Kohn, Phys. Rev. **136**, B864 (1964).
[32] G. Breit, Phys. Rev. **34**, 553 (1929); **39**, 616 (1932).
[33] O. L. Brill and B. Goodman, Am. J. Phys. **35**, 832 (1967).
[34] G. Vignale, C. A. Ullrich, and S. Conti, Phys. Rev. Lett. **79**, 4878 (1997).
[35] C. A. Ullrich and G. Vignale, Phys. Rev. B **65**, 245102 (2002).
[36] S. Conti and G. Vignale, Phys. Rev. B **60**, 7966 (1999).
[37] H. M. Böhm, S. Conti, and M. P. Tosi, J. Phys.: Condens. Matter **8**, 781 (1996).
[38] R. Nifosì, S. Conti, and M. P. Tosi, Phys. Rev. B **58**, 12758 (1998).
[39] H. Yasuhara and Y. Ousaka, Int. J. Mod. Phys. B **6**, 3089 (1992).
[40] A. J. Glick and W. F. Long, Phys. Rev. B **4**, 3455 (1971).
[41] S. Ichimaru, Rev. Mod. Phys. **54**, 1017 (1982).
[42] E. K. U. Gross and W. Kohn, Phys. Rev. Lett. **55**, 2850 (1985); **57**, 923 (1986).
[43] N. Iwamoto and E. K. U. Gross, Phys. Rev. B **35**, 3003 (1987).
[44] E. van Lenthe, E. J. Baerends, and J. G. Snijders, J. Chem. Phys. **101**, 9783 (1994).
[45] E. van Lenthe, R. van Leeuwen, E. J. Baerends, and J. G. Snijders, Int. J. Quantum Chem. **57**, 281 (1996).
[46] P. H. T. Philipsen, E. van Lenthe, J. G. Snijders, and E. J. Baerends, Phys. Rev. B **56**, 13556 (1997).
[47] F. Kootstra, P. L. de Boeij, H. Aissa, and J. G. Snijders, J. Chem. Phys. **114**, 1860 (2001).
[48] P. L. de Boeij, F. Kootstra, and J. G. Snijders, Int. J. Quantum Chem. **85**, 449 (2001).
[49] P. Romaniello and P. L. de Boeij (unpublished).
[50] G. te Velde and E. J. Baerends, Phys. Rev. B **44**, 7888 (1991); J. Comput. Phys. **99**, 84 (1992).
[51] C. Fonseca Guerra, O. Visser, J. G. Snijders, G. te Velde, and E. J. Baerends, in *Methods and Techniques in Computational Chemistry*, edited by E. Clementi and G. Corongiu (STEF, Cagliari, 1995), p. 305.
[52] G. te Velde, F. M. Bickelhaupt, E. J. Baerends, C. Fonseca Guerra, S. J. A. van Gisbergen, J. G. Snijders, and T. Ziegler, J. Comput. Chem. **22**, 931 (2001).
[53] F. Herman and S. Skillman, *Atomic Structure Calculations* (Prentice-Hall, Englewood Cliffs, NJ, 1963).
[54] E. van Lenthe and E. J. Baerends, J. Comput. Chem. **24**, 1142 (2003).
[55] G. Lehmann and M. Taut, Phys. Status Solidi B **54**, 469 (1972).
[56] G. Wiesenekker and E. J. Baerends, J. Phys.: Condens. Matter **3**, 6721 (1991); G. Wiesenekker, G. te Velde, and E. J. Baerends, J. Phys. C **21**, 4263 (1988).
[57] P. Romaniello and P. L. de Boeij, J. Chem. Phys. **122**, 164303 (2005).
[58] J. B. Smith and H. Ehrenreich, Phys. Rev. B **25**, 923 (1982).
[59] G. R. Parkins, W. E. Lawrence, and R. W. Christy, Phys. Rev. B **23**, 6408 (1981).
[60] R. T. Beach and R. W. Christy, Phys. Rev. B **16**, 5277 (1977).
[61] S. R. Nagel and S. E. Schnatterly, Phys. Rev. B **9**, 1299 (1974).